Scattering of vibrational waves in perturbed quasi-one-dimensional multichannel waveguides

A. Fellay, F. Gagel, and K. Maschke
Institut de Physique Appliquée, Ecole Polytechnique Fédérale, CH 1015 Lausanne, Switzerland

A. Virlouvet and A. Khater
Laboratoire de Physique des Matériaux, URA 807 CNRS, Université du Maine, F-72017 Le Mans Cedex, France
(Received 27 June 1996)

We investigate the scattering properties of vibrational waves in perturbed quasi-one-dimensional multichannel waveguides in the harmonic approximation. Local defects are introduced by changing the masses or the spring constants of the perfect waveguide. For both types of defects we find resonances in the continuum. These are due to the coherent coupling between local defect states and propagating states. Beyond the similarity with the quantum-mechanical case of electron scattering and associated Fano resonances, the scattering behavior of vibrational waves appears to be more complex. This complexity can be attributed to the vector character of the vibrational amplitudes and to additional possibilities for mode-mode coupling by the defects. To illustrate the method a detailed discussion of the transmission spectra is presented for the generic case of a double chain containing defects, which shows already the essential characteristic features of a multichannel system. [S0163-1829(97)05104-7]

I. INTRODUCTION

Scattering and localization phenomena in disordered low-dimensional systems have been of interest for a long time.[1] They are now of renewed interest owing to advances in technology that permit the construction of devices at the nanometric scale. Most of the recent research has been oriented towards the study of electronic scattering in quasi-one-dimensional systems, the basic motivation being to understand the limitations that structural disorder, or other kinds of disorder, may have on the physical properties of microelectronics devices.

The basis of the understanding of dc electronic transport in the mesoscopic regime and its generalization to multiterminal systems have been provided by Landauer,[2] who related the conductance of the system to its scattering matrix. More recently, several authors[3–5] have shown that multiple scattering and quantum interference become very important to describe such transport phenomena.

Scattering experiments are used in different domains of physics to investigate the physical properties of the system under consideration. Two different regimes have to be distinguished: *inelastic* and *elastic* scattering. Elastic scattering is the essential tool to investigate structural properties, limited as it is by the instrumental wavelength. X rays, for example, which are widely used for structural analysis, have their resolution limitations on the nanometric scale. Here vibrational waves could provide an interesting alternative, at least in cases where inelastic scattering probabilities due to electron-phonon and phonon-phonon scattering can be kept sufficiently small.

In the present paper we investigate the scattering of vibrational waves in perturbed crystalline quasi-one-dimensional waveguides in the harmonic approximation. While there has been interest in electronic phenomena for many years, the study of vibrational phenomena in multichannel systems has not received the attention it deserves, even though scattering in one-dimensional disordered mesoscopic atomic chains was studied.[6]

While strong similarities between electronic scattering and the scattering of vibrational waves may be expected since, mathematically speaking, we just replace the Schrödinger equation by the dynamical equation, it should be noted, however, that the case of the vibrational waves is more complicated. Here one is confronted with the scattering of vector fields described by the Cartesian amplitudes of the waves on the lattice sites, instead of scalar fields in the electronic case. Also, for the same bundle of atomic chains, the number of available channels in the vibrational case is greater than in the electronic case, which gives rise to a richer complexity.

In the following we shall demonstrate that the different nature of vibrational waves gives rise to some interesting scattering properties. As in the electron case, we find that the transmission spectra of vibrational waves can be regarded as identifying characteristics of the structural properties of the considered system. Multiple scattering becomes very important and causes a large variety of resonance features. In the language of optics or electronics these can be identified as Fabry-Pérot or as Fano resonances. In the language of mechanical vibrations at surfaces, which are considered as infinite defects terminating semi-infinite crystals, these are called continuum resonances.[7]

In Sec. II we present the dynamic and propagating characteristics of a perfect waveguide, introducing the essential features of the formalism we need later on. Section III presents the algebraic formalism for scattering at defects. In Sec. IV we give some typical examples of disordered multichannel mesoscopic systems with either mass or spring defects.

II. THE PERFECT WAVEGUIDE

A. Propagating modes

We consider the planar quasi-one-dimensional (quasi-1D) waveguide represented in Fig. 1. It consists of N_y equidistant

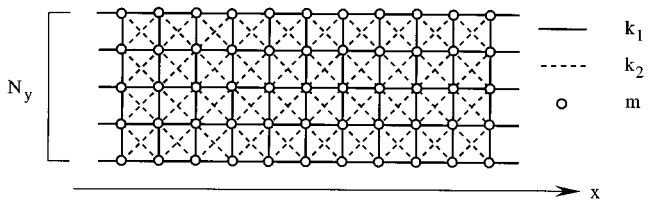

FIG. 1. Quasi-1D planar waveguide composed of N_y interconnected chains ($N_y=5$).

parallel periodic chains of masses aligned along the axis of propagation (x direction). For simplicity, the distances between adjacent masses are chosen to be the same in both the x and y directions. Each mass is linked to its nearest and next-nearest neighbors by harmonic springs with spring constants k_1 and k_2. The dynamics is described by Newton's equations leading to the corresponding dynamical equations that define the displacement amplitudes $u_{ij\alpha}$ at site (i,j) in the α direction, where $\alpha=x,y$. For bulk sites, i.e., for $2\leqslant j\leqslant N_y-1$, projection on the $x(y)$ axis yields

$$
\begin{aligned}
-m\omega^2 u_{ijx} = & -k_1(u_{ijx}-u_{i+1,j,x})-k_1(u_{ijx}-u_{i-1,j,x}) \\
& -\frac{k_2}{2}(u_{ijx}-u_{i+1,j+1,x})-\frac{k_2}{2}(u_{ijx}-u_{i+1,j-1,x}) \\
& -\frac{k_2}{2}(u_{ijx}-u_{i-1,j+1,x})-\frac{k_2}{2}(u_{ijx}-u_{i-1,j-1,x}) \\
& -\frac{k_2}{2}(u_{ijy}-u_{i+1,j+1,y})+\frac{k_2}{2}(u_{ijy}-u_{i+1,j-1,y}) \\
& +\frac{k_2}{2}(u_{ijy}-u_{i-1,j+1,y})-\frac{k_2}{2}(u_{ijy}-u_{i-1,j-1,y}), \\
-m\omega^2 u_{ijy} = & -k_1(u_{ijy}-u_{i,j+1,y})-k_1(u_{ijy}-u_{i,j-1,y}) \\
& -\frac{k_2}{2}(u_{ijy}-u_{i+1,j+1,y})-\frac{k_2}{2}(u_{ijy}-u_{i+1,j-1,y}) \\
& -\frac{k_2}{2}(u_{ijy}-u_{i-1,j+1,y})-\frac{k_2}{2}(u_{ijy}-u_{i-1,j-1,y}) \\
& -\frac{k_2}{2}(u_{ijx}-u_{i+1,j+1,x})+\frac{k_2}{2}(u_{ijx}-u_{i+1,j-1,x}) \\
& +\frac{k_2}{2}(u_{ijx}-u_{i-1,j+1,x})-\frac{k_2}{2}(u_{ijx}-u_{i-1,j-1,x}),
\end{aligned}
\tag{1}
$$

where ω is the vibration frequency. The corresponding dynamical equations for boundary sites ($j=1$ or $j=N_y$) are obtained by setting terms corresponding to absent springs to zero. Note that the diagonal springs that couple the displacements parallel and perpendicular to the x axis are necessary to stabilize the system with respect to shear.

Equations (1) must be solved for all the considered atoms with appropriate boundary conditions. In the present work we use scattering boundary conditions for which we obtain the plane-waves solutions

$$
\vec{u}^{\,i}=\vec{u}^{\,0}e^{iqx_i}, \tag{2}
$$

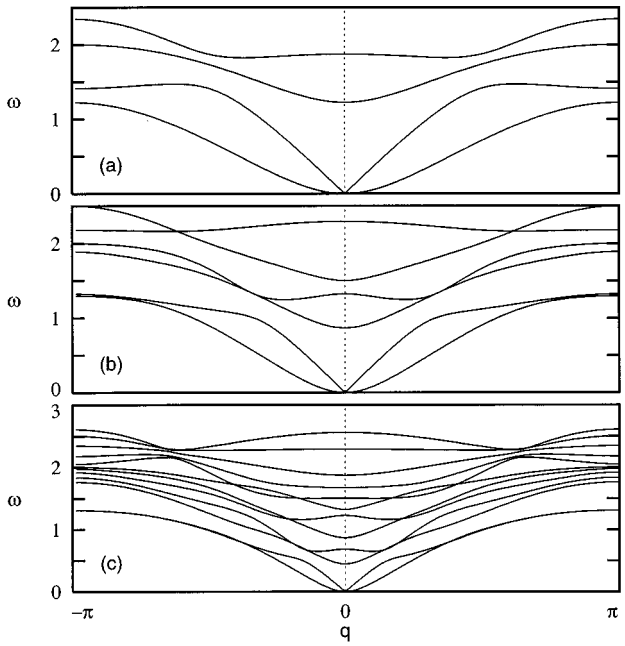

FIG. 2. Dispersion of propagating modes in planar waveguides of different widths N_y. The parameters are $k_1=1$, $k_2=0.75$, and $m=1$. (a) $N_y=2$, (b) $N_y=3$, and (c) $N_y=6$.

where q is the real wave vector, x_i denotes the equilibrium position of column i, and the vector $\vec{u}^{\,i}$ describes the displacement amplitudes of each atom in this column

$$
\vec{u}^{\,i}=\begin{pmatrix} u_{i1x} \\ u_{i1y} \\ \vdots \\ u_{iN_yx} \\ u_{iN_yy} \end{pmatrix}.
$$

For later purposes, it is convenient to relate the displacement vectors in adjacent columns by a phase factor κ, i.e., $\vec{u}^{\,i+1}=\kappa\vec{u}^{\,i}$. This phase relation is an essential feature of the matching method,[8,9] initially employed for the study of surface localized phonons and resonances. For propagating waves as in Eq. (2), we have $\kappa=e^{iqa}=e^{iq}$, assuming $a=1$. The eigenvalue problem Eq. (1) can then be written as

$$
\mathbf{C}(\kappa)\cdot\vec{u}^{\,i}=-\omega^2\vec{u}^{\,i}. \tag{3}
$$

The dynamical matrix $\mathbf{C}$ is a $2N_y\times 2N_y$ matrix. It contains terms with κ and $1/\kappa$. Solving Eq. (3) for fixed $\kappa=e^{iq}$, one obtains $2N_y$ eigenvalues ω_ν together with the corresponding eigenvectors $\vec{u}_\nu$. The propagating vibration modes of the chain correspond to solutions with $|\kappa|=1$. They are usually given in terms of q, with q running over the first Brillouin zone $[-\pi,\pi]$. In the considered 2D case we have two acoustical modes with $\omega\to 0$ for $q\to 0$, the remaining modes being optical with ω different from zero for all q. Figure 2 shows the dispersion curves for different numbers of chains using the parameters $k_1=1$, $k_2=0.75$, and $m=1$. These parameters will be systematically used in all our following numerical calculations. It is seen that the dispersion becomes

already complicated even for these simple cases. This would naturally be even more so for increasing N_y, since the number of modes grows simultaneously. The eigenmodes of the waveguide are either symmetric or antisymmetric with respect to the central axis in the x direction. Symmetric modes correspond to atomic displacements that satisfy the conditions

$$u_{ijx} = u_{i,N_y+1-j,x} \quad ,$$

$$u_{ijy} = -u_{i,N_y+1-j,y} \quad ,$$

whereas for the antisymmetric modes the displacements satisfy

$$u_{ijx} = -u_{i,N_y+1-j,x} \quad ,$$

$$u_{ijy} = u_{i,N_y+1-j,y} \quad .$$

In the case of the double chain we have one acoustical and one optical mode for each symmetry. The anticrossing behavior between the symmetric acoustical and optical modes observed in Fig. 2 is due to the fact that dispersion curves belonging to the same symmetry interact and therefore do not cross. Note further that the antisymmetric transverse acoustic mode has a q^2 dispersion for $q \to 0$. This behavior is a consequence of the finite extension of the waveguide in the y direction (see, e.g., Ref. 10 for the continuum case).

B. Evanescent modes

In order to describe the scattering in presence of defects, we not only have to know the propagating modes described above, but also to consider the evanescent solutions for the multichannel system. In other words, for a given ω, we need all the solutions κ, including those with $|\kappa_\nu| \neq 1$. These solutions can be obtained using different procedures.[9,11,12] An elegant and well suited way is given (see Ref. 13 for the similar electronic problem) by introducing new unknowns $v_{ij\alpha}$ defined by

$$v_{ij\alpha} = -\frac{1}{\kappa} u_{ij\alpha}. \tag{4}$$

We then can rewrite Eq. (3) in the form of an eigenvalue problem for κ,

$$\mathbf{A}(\omega) \cdot \vec{W} = \kappa \mathbf{B} \cdot \vec{W} \quad \text{with} \quad \vec{W} = \begin{pmatrix} \vec{u}^i \\ \vec{v}^i \end{pmatrix}. \tag{5}$$

Note that the dimension of this generalized eigenvalue problem is twice as large as the original problem.

The solution of Eq. (5) yields N_y pairs of eigenvalues κ_ν and $1/\kappa_\nu$. As discussed above, eigenvalues with $|\kappa_\nu| = 1$ correspond to propagating waves, which are described by real wave vectors q. These solutions may be grouped into pairs corresponding to the two directions of propagation. Both solutions are linked by time-reversal symmetry. Since each of the two solutions contains the same information, we consider in the following only waves propagating from the left to the right. Solutions with $|\kappa_\nu| \neq 1$ correspond to evanescent or divergent waves. Only the physically relevant evanescent modes are retained. Both propagating and evanescent solutions are needed to describe the scattering solutions in the presence of defects.

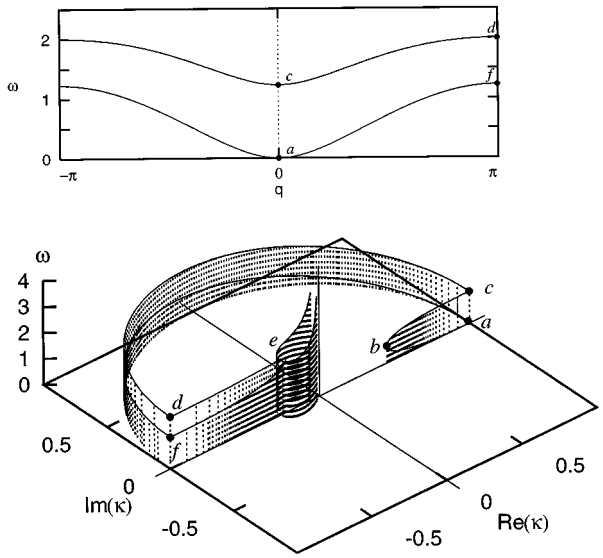

FIG. 3. Functional behavior $\omega(\kappa)$ of the antisymmetric modes in a double chain. For comparison, the dispersion curves $\omega(q)$ for the corresponding propagating modes are shown on top.

The functional behaviors of the symmetric and antisymmetric eigenmodes in the κ plane are given in Figs. 3 and 4 for the case of the double chain. As mentioned above, the propagating modes of Fig. 2 are represented by the curves following the unit circle in the κ plane. In order to show the correspondence between Fig. 2 and Figs. 3 and 4, we have also reproduced the dispersion curves $\omega(q)$ for the respective symmetries considered in Figs. 3 and 4. To facilitate the comparison, we have marked common special points in both the $\omega(\kappa)$ and the $\omega(q)$ representations.

The functional behavior of the modes, corresponding to the solutions on and inside the unit circle in Figs. 3 and 4,

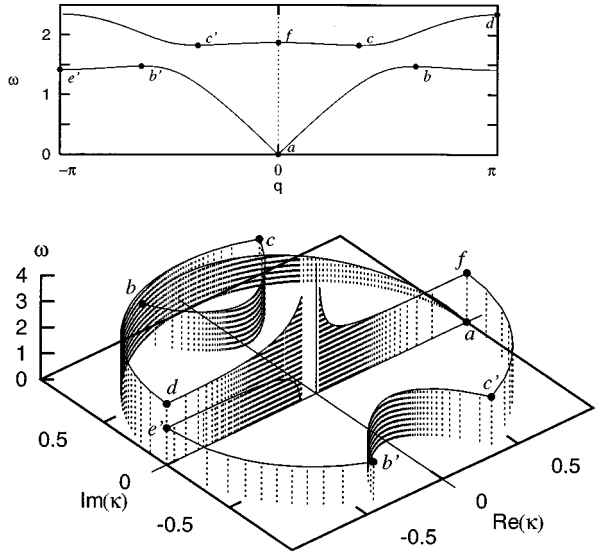

FIG. 4. Functional behavior $\omega(\kappa)$ of the symmetric modes in a double chain. For comparison, the dispersion curves $\omega(q)$ for the corresponding propagating modes are shown on top.

turns out to be rather intricate. Consider first the two antisymmetric modes in the three-dimensional view of Fig. 3. Both are degenerate at point a ($\kappa=1$, $\omega=0$). For increasing ω, one solution is the acoustical dispersion branch up to point f at $\omega=\omega_f$ and $\kappa=-1$; it becomes evanescent for larger ω. The other solution is associated with the optical mode. Starting from a, it is immediately evanescent at small frequencies, passes through a minimum of κ ($\kappa_{\min}=0.45$) at b ($\omega=0.64$), joins again the unit circle at c ($\kappa=1$), and becomes the propagating optical dispersion branch up to d ($\kappa=-1$), before becoming evanescent again. For still higher frequencies ($\omega>\omega_d$), both solutions follow first the negative real κ axis up to e, where they become degenerate, and then they split up again, remaining evanescent but with complex κ and $|\kappa|\to 0$ for $\omega\to\infty$. We will see later that the rather complicated functional behavior of the evanescent solution in the range of acoustical modes $0<\omega<1.25$ (path $a\to b\to c$), including the degeneracy with the other solution at point a, is at the origin of some interesting scattering properties in this frequency range.

For the symmetric modes, the functional behavior in the complex κ plane is shown in Fig. 4. It is even somewhat more complicated than that for the antisymmetric modes. This is essentially due to the anticrossing behavior of the propagating modes, which was already mentioned above. The solution starting at point a follows the propagating acoustical mode up to point b, which corresponds to the maximum frequency in this branch. It then joins the minimum of the optical branch at point c through an evanescent path with $|\kappa|\neq 1$. From c to d it continues on the propagating optical branch, before becoming again evanescent with real negative κ. The second solution is evanescent for $\omega=0$, starting with a real negative value of κ. For increasing ω it follows the negative κ axis, to reach point e' in the propagating optical branch, continues on this propagating branch up to its maximum frequency at point b', and then joins the point c' on the propagating optical branch via an evanescent path. It coincides with the propagating optical branch between points c' and f and then becomes evanescent with real positive κ. For higher frequencies both solutions remain evanescent with $|\kappa|\to 0$ for $\omega\to\infty$.

III. SCATTERING AT DEFECTS

We now consider a waveguide perturbed by defects. The situation is depicted in Fig. 5. The perturbed region M extends over columns 0 to N. To its left (L) and right (R) it is attached to two unperturbed semi-infinite waveguides. Since the perfect waveguides do not couple between different eigenmodes, we can treat the scattering problem for each eigenmode separately. For an incoming wave in eigenmode $\overline{\nu}$,

$$\vec{u}^{\,i}_{\rm in}=(\kappa_{\overline{\nu}})^i\vec{u}_{\overline{\nu}},\quad i\leqslant -1, \tag{6}$$

the resulting scattered waves are composed of a reflected and a transmitted part, which can be expressed as a superposition of the eigenmodes of the perfect waveguide at the same frequency, i.e.,

$$\vec{u}^{\,i}_r=\sum_\nu\ \xi_{\nu\overline{\nu}}(\kappa_\nu^{-1})^i\vec{u}_\nu(\kappa_\nu^{-1}),\quad i\leqslant -1 \tag{7}$$

$$\vec{u}^{\,i}_t=\sum_\nu\ \eta_{\nu\overline{\nu}}(\kappa_\nu)^i\vec{u}_\nu(\kappa_\nu),\quad i\geqslant N+1. \tag{8}$$

The coefficients $\xi_{\nu\overline{\nu}}$ and $\eta_{\nu\overline{\nu}}$ determine the reflection and transmission coefficients (see below). With the definitions Eqs. (7) and (8), we can rewrite the dynamical equations for the perturbed chain. Since there are perfect waveguides in regions L and R, we only need to solve Eqs. (1) for the masses inside the perturbed zone M and in the boundary columns -1 and $N+1$, which are matched to the rest of the perfect waveguide by Eqs. (7) and (8). This yields a linear system of equations with $2N_y(N+3)$ unknowns, namely, the $2(N+1)N_y$ displacement amplitudes $u_{ij\alpha}$ of the perturbed region M and the $4N_y$ coefficients $\xi_{\nu\overline{\nu}}$ and $\eta_{\nu\overline{\nu}}$. Isolating the inhomogeneous terms describing the incoming wave, we obtain an inhomogeneous system of linear equations

$$\tilde{\mathbf{D}}(\omega)\cdot\vec{x}=-\vec{y}(\omega) \tag{9}$$

or, expanding the expressions,

$$\begin{pmatrix}
D_{LL} & D_{LM} & 0 & \cdots & \cdots & \cdots & \cdots & 0\\
D_{ML} & D_{M_{00}} & D_{M_{01}} & 0 & & & & \vdots\\
0 & D_{M_{10}} & D_{M_{11}} & D_{M_{12}} & 0 & & & \vdots\\
\vdots & \ddots & \ddots & \ddots & \ddots & \ddots & & \vdots\\
\vdots & & \ddots & \ddots & \ddots & \ddots & \ddots & \vdots\\
\vdots & & & 0 & D_{M_{N-1,N-2}} & D_{M_{N-1,N-1}} & D_{M_{N-1,N}} & 0\\
\vdots & & & & 0 & D_{M_{N,N-1}} & D_{M_{NN}} & D_{MR}\\
0 & \cdots & \cdots & \cdots & \cdots & 0 & D_{RM} & D_{RR}
\end{pmatrix}
\begin{pmatrix}
\vec{\xi}_{\overline{\nu}}\\ \vec{u}^{\,0}\\ \vec{u}^{\,1}\\ \vdots\\ \vdots\\ \vec{u}^{\,N-1}\\ \vec{u}^{\,N}\\ \vec{\eta}_{\overline{\nu}}
\end{pmatrix}
=-\begin{pmatrix}
\vec{F}\\ \vec{G}\\ 0\\ \vdots\\ \vdots\\ 0\\ 0
\end{pmatrix}. \tag{10}$$

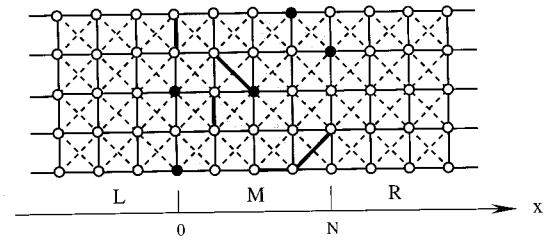

FIG. 5. Perturbed planar quasi-1D waveguide. The perturbed region (shaded) contains defect masses (full dots) and defect springs (thick lines).

In our model, the system contains only interactions between adjacent columns. The matrix $\tilde{\mathbf{D}}$ is consequently tridiagonal by blocks. Each of the off-diagonal $2N_y \times 2N_y$ blocks describes the coupling between adjacent columns. The block matrices as well as the vectors $\vec{F}$ and $\vec{G}$ are given in the Appendix. It is easy to see that mass defects change only the diagonal blocks $D_{M_{ii}}$, while defects in the spring constants may enter anywhere in the $D_{M_{ij}}$ $(j=i,i\pm 1)$.

The solutions of Eq. (10) yield the displacements $u_{ij\alpha}$ of the atoms in the perturbed region as well as the coefficients $\xi_{\nu\bar{\nu}}$ and $\eta_{\nu\bar{\nu}}$, which determine the displacements of the atoms in the unperturbed regions L and R of the waveguide. The scattering behavior is usually described in terms of the scattering matrix. Its elements are given by the relative transmission or reflection amplitudes $\tau_{\nu\bar{\nu}}$ and $\rho_{\nu\bar{\nu}}$ of the scattered waves in mode ν for an incoming wave in mode $\bar{\nu}$. In order to obtain unitarity of the scattering matrix, the scattered waves have to be normalized with respect to their group velocity. In the following, we concentrate on the discussion of the transmission and reflection probabilities. They are given by the absolute squares of the respective elements of the scattering matrix. Explicitly, for waves incoming in mode $\bar{\nu}$, the reflection probabilities are

$$r_{\nu\bar{\nu}}=|\rho_{\nu\bar{\nu}}|^2=\frac{v_\nu}{v_{\bar{\nu}}}|\xi_{\nu\bar{\nu}}|^2 \tag{11}$$

and the transmission probabilities

$$t_{\nu\bar{\nu}}=|\tau_{\nu\bar{\nu}}|^2=\frac{v_\nu}{v_{\bar{\nu}}}|\eta_{\nu\bar{\nu}}|^2. \tag{12}$$

Here v_ν is the group velocity in channel ν, which is set equal to zero for evanescent modes. The evanescent modes are necessary for a complete description of the overall dynamics and of the scattering amplitudes of the multichannel waveguide, although they do not contribute to energy transport.

In order to characterize the overall transmission of mesoscopic disordered multichannel systems at a given frequency ω, it is useful to define a total transmission Λ by summing over all input and output channels

$$\Lambda(\omega)=\sum_{\nu,\bar{\nu}} t_{\nu\bar{\nu}}, \tag{13}$$

where the sum is carried out over all propagating modes at frequency ω. The total transmission is important for calculating experimentally measurable quantities. For example, in full analogy with the Landauer description of electron transport, we obtain for the energy current between two heat baths held at slightly different temperatures T_1 and T_2

$$I_E=\frac{k_B^2 T}{h}\int_0^\infty dx\, x^2 \Lambda\left(\frac{k_B T x}{\hbar}\right)\frac{e^x}{(e^x-1)^2}(T_1-T_2), \tag{14}$$

with $T_1 \leqslant T \leqslant T_2$. Division by (T_1-T_2) yields the heat conductance.

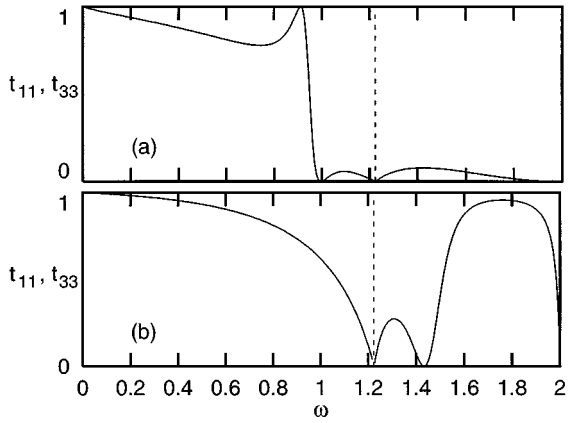

FIG. 6. Transmission probabilities for the antisymmetric modes in a double chain containing two mass defects $m_1=m_2=M$. (a) $M=3$ and (b) $M=0.3$.

IV. RESULTS AND DISCUSSION

A. Mass defects in a double chain

The simplest multichannel configuration to study is the double chain with mass defects. In what follows, the subscripts on $t_{\nu\nu'}$ refer to Fig. 2(a), where the modes are numbered 1–4 from bottom to top. We first consider a local symmetric mass defect on one column, described by the defect masses $m_1=m_2=M$ on the two column sites. Modes of different symmetry are not coupled. Since both symmetric and antisymmetric modes show qualitatively the same behavior, we show only the transmission spectrum of the antisymmetric modes in Fig. 6. The presence of defects leads to a general decrease of the transmission probability. As expected, the influence of the defects is smallest in the acoustical regime. For $\omega \to 0$ we get $t_{11} \to 1$, independent of the perturbation. A general behavior is observed, namely, that backscattering becomes most important for q vectors near the zone boundaries (vertical broken line), where we get $t_{11}, t_{33} \to 0$, independent of the strength of the defect. A second observed feature, which is defect specific, manifests itself in strong asymmetric resonances. These can be attributed to the presence of defect-induced resonant states, whose frequency depends on the defect mass. This dependence can be easily understood in a simple picture. Defects with $M>m$ give rise to bound states below the optical modes, whereas defects with $M<m$ lead to local modes with frequencies larger than the maximum frequencies of the acoustical or the optical modes. The presence of these bound states in the frequency range of the propagating states leads to the additional resonances in the transmission spectra observed in Fig. 6, which thus can be identified as Fano-like resonances. The situation is quite similar to the case of electron waveguides discussed in Ref. 5. In the latter case it was possible to de-

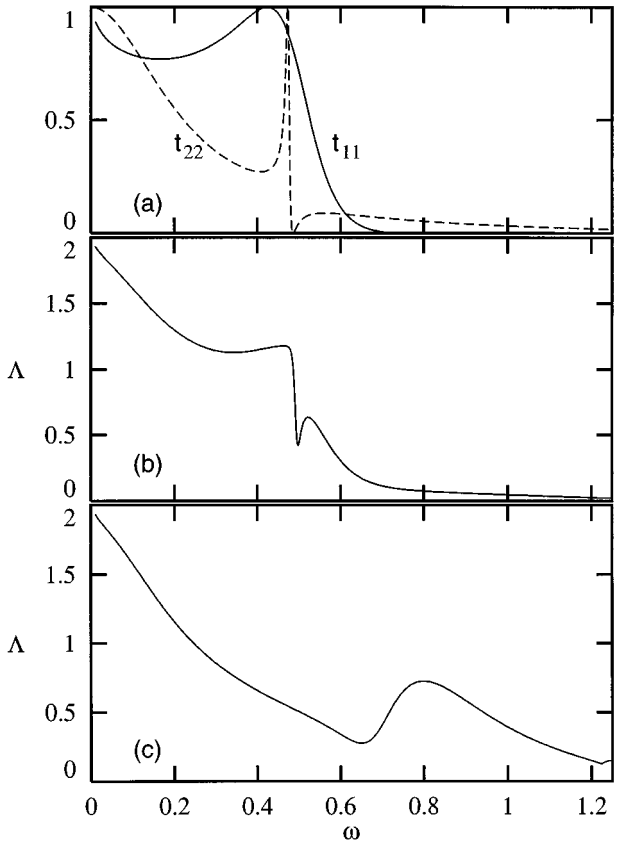

FIG. 7. Influence of the asymmetry of a nonsymmetric local defect on the total transmission Λ in a double chain. The total mass of the defect is $M_{\mathrm{tot}}=m_1+m_2=22$; the asymmetry parameter α is given by $\alpha=m_1-m_2$. (a) Transmission probabilities t_{11} (antisymmetric acoustic mode) and t_{22} (symmetric acoustic mode) for $\alpha=0$, (b) total transmission Λ for $\alpha=6$, and (c) total transmission Λ for $\alpha=16$.

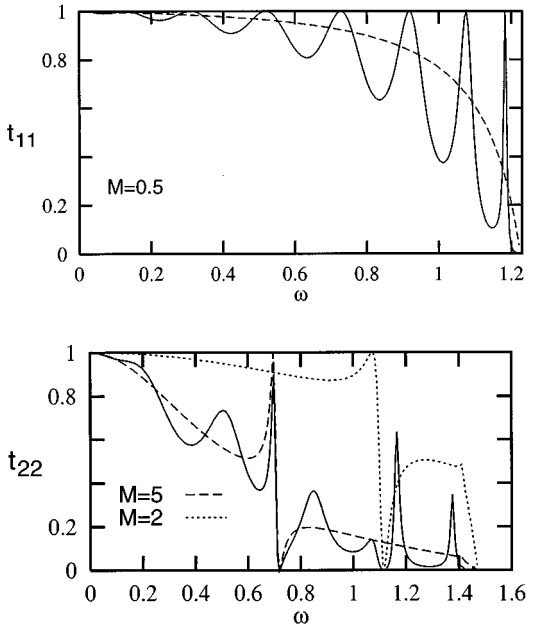

FIG. 8. Transmission probabilities for two columns of symmetric mass defects at distance N between each other. The dashed lines show the transmission probabilities for the single defects. (a) t_{11} (acoustical antisymmetric mode) for $M=0.5$ and $N=8$ and (b) t_{22} (acoustical symmetric mode) for two different symmetric defects at distance $N=8$. The defect masses are $M_1=2$ and $M_2=5$, respectively.

scribe the position of the transmission zeros analytically. In the present situation of vibrational waves, however, each site possesses already two degrees of freedom and the dimension of the system of linear equations [see Eq. (10)] becomes twice as large. In the simplest possible case of a symmetric local mass defect in a double chain the dimension of the system is equal to 6 and it is already impossible to obtain compact analytical expressions for the scattering coefficients or the positions of the transmission zeros.

As may be expected from the above arguments, the resonances shift to higher (lower) frequencies for smaller (larger) defect masses. We note that for $M<m$ the transmission probability of the optical mode near the resonance does not reach unity, as is usually the case. This fact can be attributed to the interaction between the optical and the acoustical modes, which has no analog in the electronic waveguide discussed in Ref. 5.

Defects composed of two different masses in one column of the waveguide break the axial symmetry along the waveguide. This leads to additional coupling between symmetric and antisymmetric modes. It is convenient to describe such defects by the total defect mass $M_{\mathrm{tot}}=m_1+m_2$ and the asymmetry parameter $\alpha=m_1-m_2$. In Fig. 7 we show our numerical results for the total transmission $\Lambda=\Sigma_{\nu,\bar{\nu}}t_{\nu\bar{\nu}}$, $\nu,\bar{\nu}=1,2$, with $M_{\mathrm{tot}}=22$ and two different α values. For comparison we also give the transmission behavior of modes 1 (antisymmetric) and 2 (symmetric) when $m_1=m_2$, showing the expected resonances. It is seen that for an intermediate value of the asymmetry parameter ($\alpha=6$) the single sharp resonance of t_{22} that exists for $\alpha=0$ can still be resolved in the Λ spectrum; a further increase of α ($\alpha=16$) leads to a strong enhancement of the t_{11} resonance in the spectrum, but suppresses the t_{22} resonance. It is interesting to note that in the frequency region $0.6<\omega<1.2$ this α-induced coupling leads to a rather strong increase of the total transmission Λ, far beyond its value of $t_{11}+t_{22}$ at $\alpha=0$.

Up to now we have considered defects that are localized on one column. For a distribution of such defects we expect additional Fabry-Pérot oscillations due to the interference between multiply scattered waves. In Fig. 8 we show the transmission probabilities for the system of two separated symmetric defects and for the acoustic symmetric and antisymmetric modes. In both cases we find Fabry-Pérot oscillations depending on the distance between the defects. The presented transmission spectrum for the symmetric acoustical mode (bottom of Fig. 8) shows also the supplementary Fano-like resonances caused by the single defects. None of these are present in the presented transmission spectrum for the antisymmetric acoustical mode (top of Fig. 8), since in the chosen example the respective eigenfrequencies of the local defects are positioned above the acoustical mode.

Figure 9 shows the transmission spectrum of the antisymmetric acoustical mode for a sequence of five equally spaced columns of defects, with masses $m_1=m_2=2$. Here the Fabry-Pérot oscillations lead to a splitting into separate bands of high transmission probability, which are correlated with the distance d between adjacent defects ($d=3$ in this case), whereas the small oscillations within these windows

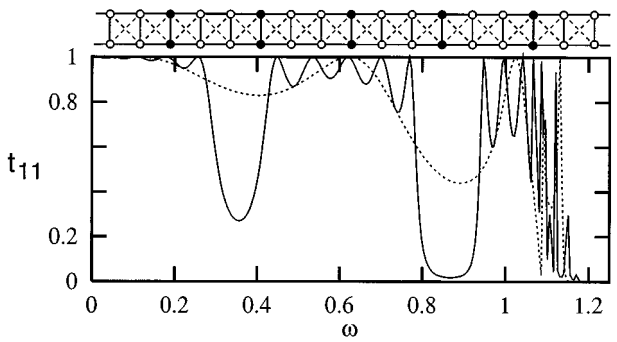

FIG. 9. Transmission probability for the acoustical antisymmetric mode for a sequence of five equidistant symmetric local mass defects. The defect structure is shown on top. The masses at the full points are $m_1=m_2=2$. The dashed line gives the transmission probability for two defects with the same spacing.

depend directly on the full width of the defect region ($N=12$). The rapid oscillations in the frequency range $1<\omega<1.2$ are due to the resonances caused by the defect-induced resonant states attached to the symmetric optical mode.

B. Spring defects in a double chain

Defects can also be introduced by changing some springs in the waveguide. Unlike mass defects, the spring defects act simultaneously on two sites. One can therefore expect some new features in the transmission spectra. In the following we concentrate on some examples of simple spring defects in the double chain that reveal already their somewhat particular nature.

The simplest defect is obtained by replacing one of the vertical spring constant k_1 by g. We find that the transmission of the antisymmetric mode is not affected by the defect. In fact, for this symmetry, both atoms in a column move by the same distance in the y direction, whereas they move in the opposite direction along the x axis. Therefore, the vertical springs are not used for either the y motion, which does not change the distance between the two masses, or the x motion, since there is no *harmonic* contribution to the restoring force. The transmission spectrum for the symmetric acoustical mode, in contrast, is shown in Fig. 10. Here, both atoms move in the opposite direction along the y axis and thus the replaced vertical spring contributes. For $g<k_1$ this leads to the resonance behavior in the acoustic regime seen in Fig. 10.

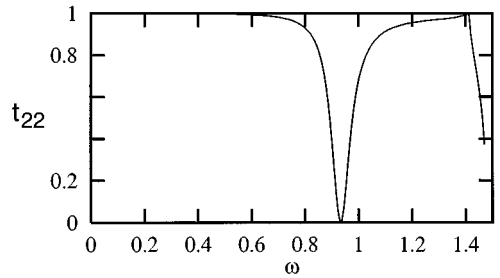

FIG. 10. Transmission probability for the acoustical symmetric mode for changed vertical spring. The spring constant of the new spring is $g=0.2k_1$.

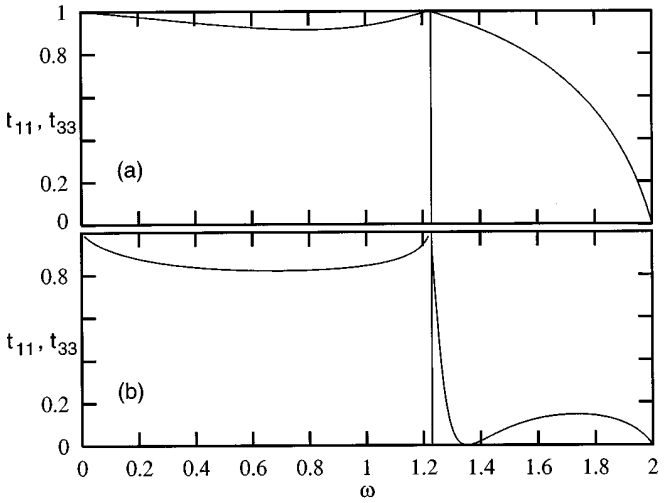

FIG. 11. Transmission probability for the antisymmetric mode for a local symmetric change of the horizontal springs. The vertical lines indicate the border of the bands. The spring constant of the new springs is g. (a) $g=10k_1$ and (b) $g=0.2k_1$.

The influence of the horizontal springs on the transmission behavior of the antisymmetric modes is shown in Figs. 11(a) and 11(b). Here we have replaced both horizontal springs between two adjacent columns by springs with the constant g, thus preserving the axial symmetry of the waveguide. For large g [see Fig. 11(a)] the transmission in the acoustical regime remains nearly unaltered, whereas the transmission in the optical band decays monotonically and vanishes at the maximum frequency of the optical branch. Even for $g<k_1$ [see Fig. 11(a)], the transmission probability in the acoustical branch does not change very much and remains close to unity. However, in the optical-frequency regime we obtain a resonance. This is different for the symmetric modes, where no resonances can be observed in the transmission spectra, regardless of the strength of the replaced spring; i.e., apparently these defects are always too weak to give rise to resonant states in the frequency domains of the symmetric propagating modes. A typical transmission spectrum for the symmetric modes in this case is shown in Fig. 12. Apart from rather sharp minima near the band edges at the top of the acoustic branch and the bottom of the optical band, the transmission probability decreases monotonically with increasing frequency.

The effect of changing both oblique springs at one position is shown in Fig. 13 for the antisymmetric modes and for

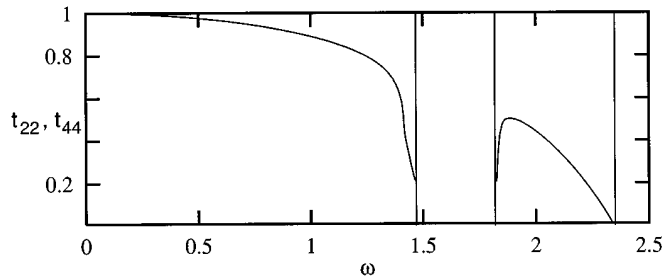

FIG. 12. Transmission probability for the symmetric modes for a local symmetric change of the horizontal springs. The spring constant of the new springs is $g=0.5k_1$. The vertical lines indicate the border of the bands.

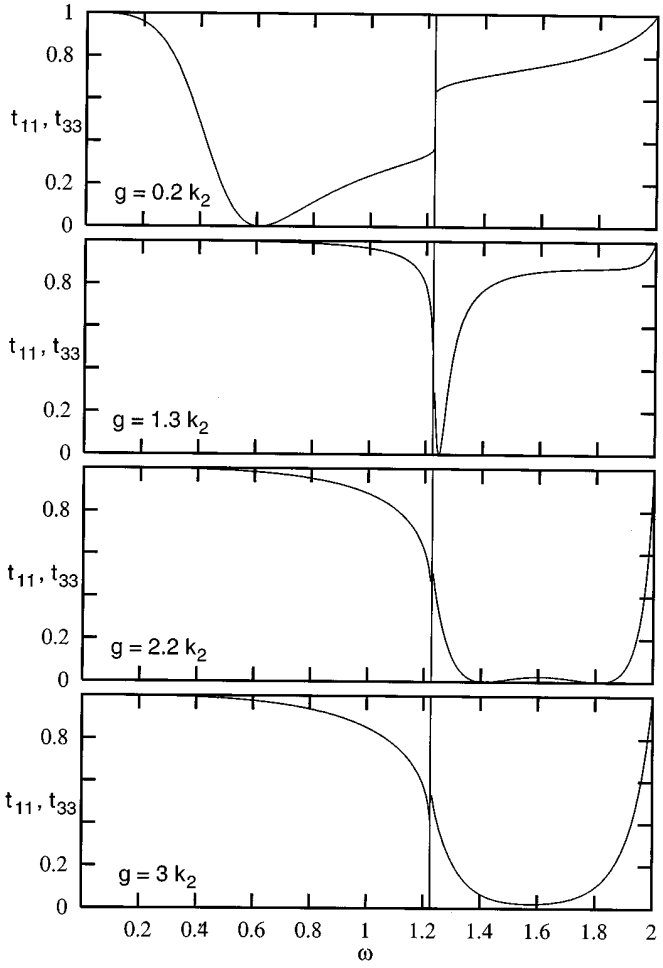

FIG. 13. Transmission probability for the antisymmetric modes for symmetric local changes of both oblique spring constants. The spring constant of the new springs is g. The vertical line indicates the border of the bands.

a series of spring constants. As may be expected, spring constants $g<k_2$ lead to a Fano-like resonance in the acoustical regime and the resonance frequency increases with g. Similarly, for g slightly larger than k_2 (see case $g=1.3k_2$ in Fig. 13), this resonance is found at the bottom of the optical mode. Quite surprisingly, increasing g even more, we obtain a second resonance structure in the upper frequency range of the optical mode (see case $g=2.2k_2$ in Fig. 13), which is apparently due to the appearance of a second resonant state in this region. Both resonances approach each other with increasing g and become degenerate at $g=2.5k_2$. Beyond

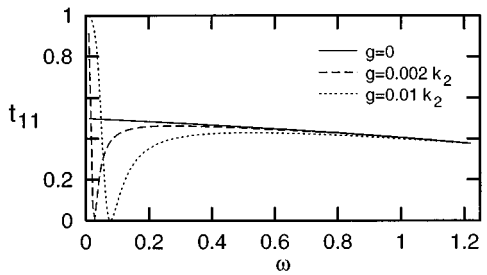

FIG. 14. Transmission probability for the antisymmetric acoustical mode for different local symmetric oblique-spring defects for $g\rightarrow 0$.

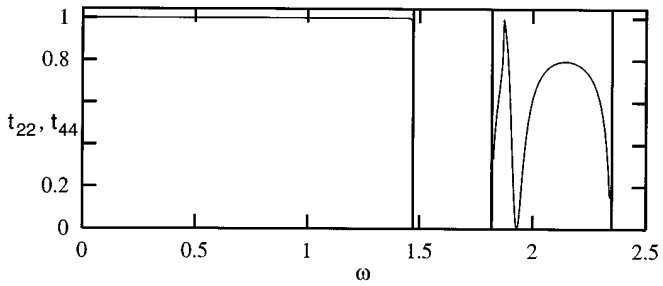

FIG. 15. Transmission probability for the symmetric modes for a symmetric oblique-spring defect with $g=1.3k_2$. The vertical lines indicate the border of the bands.

this value no transmission zero is found (see, e.g., case $g=2.2k_2$ in Fig. 13), but the transmission remains strongly suppressed in the center of the optical regime.

A rather curious behavior is also found for the transmission spectrum of the antisymmetric acoustical modes. For symmetric oblique-spring defects with $g\rightarrow 0$, which correspond to a local instability against shear motion, the transmission probability remains strongly affected even in the limit of extremely low frequencies and approaches 1/2 rather than unity when $\omega\rightarrow 0$ (see Fig. 14). This behavior seems rather strange since, in general, the transmission of sound in the low-frequency regime is expected not to be hindered by local defects. It can, however, be explained if we remember the special $\kappa(\omega)$ functional behavior of the antisymmetric modes in the low-frequency range. In the limit $\omega\rightarrow 0$, there are two modes, one propagating and the other evanescent, but with $\kappa\rightarrow 1$. In other words, the evanescent mode becomes more and more extended and at $\omega=0$ it is degenerate with the acoustical propagating mode. Since, strictly speaking, transmission is only possible through propagating states, the transmission probability remains approximately equal to 1/2 at small but finite frequencies. Experimentally one would need, however, an infinite waveguide to measure this kind of effect.

The effect of symmetric oblique-spring defects on the symmetric modes is shown in Fig. 15. The transmission re-

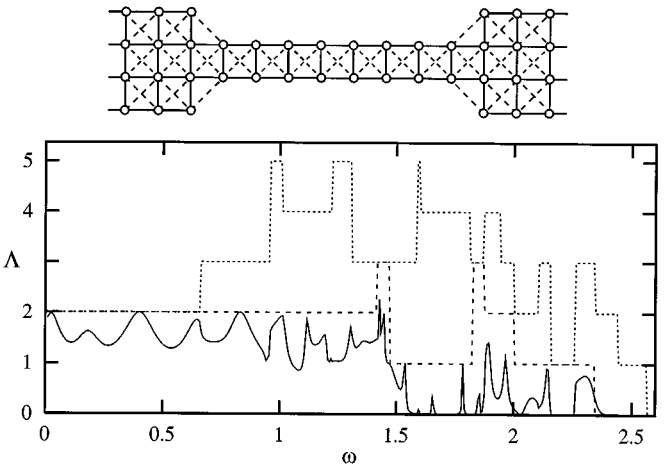

FIG. 16. Total transmission through the constriction with the geometry shown on top. The dashed (dotted) lines show the transmission probabilities of the perfect waveguides consisting of two (four) chains.

mains nearly perfect in the acoustical branch. For $g > k_2$ we observe a resonance in the optical band, which shifts to higher frequency with increasing g.

C. Transmission through a constriction

In the previous sections we have discussed the effect of perturbations on the transmission of vibrational waves in a double chain. The numerical calculations can easily be extended to a wider class of systems including a larger number of coupled chains. In this case, it is convenient to discuss the total transmission rather than the transmission probabilities for single specific modes. The results are qualitatively the same as for the double chain. In particular, the transmission spectra can be understood in terms of Fabry-Pérot and Fano-like resonances. There is, of course, a great variety of defects that cannot be discussed in detail in this paper. In Fig. 16 we show the Λ spectrum for the most simple case of a constriction in a waveguide consisting of four chains. For comparison, we also show the total transmission spectra for the two ideal waveguides consisting of four or two chains, respectively. The oscillations in the low-frequency regime ($\omega < 1$) can be related to Fabry-Pérot oscillations due to interference between multiply reflected waves at the junctions; the sharp structures observed at higher frequencies are essentially caused by resonances involving local states near the band edges.

V. CONCLUSION

In the present paper we have developed an approach that allows us to treat the scattering of vibrational waves in multichannel quasi-one-dimensional disordered mesoscopic systems in an efficient manner by solving the dynamical equations directly for scattering boundary conditions. Even though the presented method is inspired by previous work on electron waveguides, it should be emphasized that the case of vibrational waves, which has not yet been treated in the literature, is more complicated than the electron case, the essential difference being that the wave functions in the Schrödinger equation are complex *scalars*, whereas the vibrational amplitudes are complex *vectors*. In this sense, our present work provides a basis for the study of interference phenomena involving other polarizable vector waves, e.g., electromagnetic waves. In fact, defect-induced mode coupling between propagating modes plays an important role in the theory of electromagnetic waveguides and has been the object of many investigations. In particular, in the microwave regime, Fano-type interference resonances are commonly used to build filters.[14] At optical frequencies, however, interference effects are washed out due to the strong coupling between the guided electromagnetic waves and the radiation modes outside the waveguide.[15]

While we have restricted our present discussion to the case of planar waveguides, our approach can be extended in a straightforward manner to describe quasi-1D waveguides of finite size in the y and z directions. This would be useful for calculation of the transmission spectra of realistic systems, although we do not expect marked differences with the planar case. This algebraic approach can also be generalized in principle to the scattering of vibrational waves in two-dimensional infinite structures having a certain crystalline thickness, following Ref. 12, which generalizes the matching procedure to such systems.

Our numerical results for the case of a double chain show that in spite of their different character, the scattering of vibrational waves has some features in common with the scattering of electron waves and can be described in terms of basically the same interference phenomena, namely, Fabry-Pérot oscillations and Fano-like resonances. It should be noted that both phenomena are based on the same basic mechanism, namely, the interferences between multiply reflected waves in the perturbed region, the essential difference being that Fabry-Pérot oscillations involve multiple scattering of propagating states, whereas Fano resonances are usually evoked to describe the interference between a propagating transmitted mode and a local defect mode, which itself matches the evanescent states of the waveguide. It is hence evident that the evanescent modes are necessary for a complete description of the overall dynamics and of the scattering amplitudes in a multichannel system, although they do not contribute to energy transport. The transmission spectra can thus be regarded as identifying features of the specific defect structures and may therefore be used for their characterization.

Electron scattering is of fundamental importance for the understanding of dc-transport properties. Experimental investigations of the scattering properties of electrons at the Fermi energy are rather easy, provided the contact problem has been solved. The energy dependence of the transmission spectra is, however, difficult to measure, since the Fermi energy of the sample can only be varied in a very limited range.

In analogy, vibrational waves are responsible for the heat transport in insulators. In this case, it is straightforward to express the heat conductance in terms of the transmission probabilities of the vibrational waves [see Eq. (14)]. The essential difference with electrons is that phonons obey the Bose-Einstein statistics and therefore the conductance is given by a weighted average of the transmission probabilities over the full frequency range rather than by the transmission probability at a single frequency. For this reason, heat-conductance measurements are not well suited to study the transmission spectrum for vibrational waves. While measurements of mode-specific transmission probabilities will be rather difficult, direct measurements of the total transmission spectrum $\Lambda(\omega)$ should be feasible. The experimental challenge would be to couple a receiver and an emitter with known frequency characteristics to the ends of a waveguide avoiding backreflections at the junctions.

It should be noted that the interference phenomena discussed in this paper are derived from the dynamical equations, which can be applied to any length scale provided that phase coherence is not destroyed by dissipative effects. Depending on the system and on the frequency range, the phase coherence of vibrational waves can often be kept rather large. In other words, our results for the transmission spectra of vibrational waves are not limited to the nanometer scale, as is the case for coherent electron scattering, but may also describe defect-induced interference effects in macroscopic systems.

ACKNOWLEDGMENT

Part of this work was supported by the Swiss National Science Foundation under Grant No. 21-45253.95.

APPENDIX: EXPLICIT FORM OF THE SCATTERING EQUATIONS EQ. (10)

The matrix $\tilde{\mathbf{D}}$ in Eq. (10) is block tridiagonal. It is composed of the $2N_y \times 2N_y$ matrices $D_{M_{ii}}$, $D_{M_{ii\pm1}}$ $(i=0,\ldots,N)$, D_{LL}, D_{LM}, D_{ML}, D_{MR}, D_{RM}, and D_{RR}, which are all tridiagonal themselves. In the following we consider only mass defects, i.e., all springs are supposed to be the same as in the perfect wave guide. The blocks $D_{M_{i,i+1}}$ and $D_{M_{i+1,i}}$, which describe the interaction between adjacent columns, are then given by

$$D_{M_{i,i+1}} = V_{\text{up}} = \begin{pmatrix} K_1 & K_{2+} & 0 & \cdots & \cdots & 0 \\ K_{2-} & K_1 & K_{2+} & 0 & & \vdots \\ 0 & K_{2-} & K_1 & K_{2+} & \ddots & \vdots \\ \vdots & \ddots & \ddots & \ddots & \ddots & 0 \\ \vdots & & 0 & K_{2-} & K_1 & K_{2+} \\ 0 & \cdots & \cdots & 0 & K_{2-} & K_1 \end{pmatrix} \tag{A1}$$

and

$$D_{M_{i+1,i}} = V_{\text{down}} = \begin{pmatrix} K_1 & K_{2-} & 0 & \cdots & \cdots & 0 \\ K_{2+} & K_1 & K_{2-} & 0 & & \vdots \\ 0 & K_{2+} & K_1 & K_{2-} & \ddots & \vdots \\ \vdots & \ddots & \ddots & \ddots & \ddots & 0 \\ \vdots & & 0 & K_{2+} & K_1 & K_{2-} \\ 0 & \cdots & \cdots & 0 & K_{2+} & K_1 \end{pmatrix}, \tag{A2}$$

with

$$K_1 = \begin{pmatrix} k_1 & 0 \\ 0 & 0 \end{pmatrix},$$

$$K_{2+} = \begin{pmatrix} \frac{k_2}{2} & \frac{k_2}{2} \\ \frac{k_2}{2} & \frac{k_2}{2} \end{pmatrix},$$

and

$$K_{2-} = \begin{pmatrix} \frac{k_2}{2} & -\frac{k_2}{2} \\ -\frac{k_2}{2} & \frac{k_2}{2} \end{pmatrix}.$$

For the diagonal blocks containing the masses we obtain similarly

$$D_{M_{i,i}} = V_{\text{auto}} + \omega^2 \mu_i \cdot \mathbf{1} = \begin{pmatrix} P & T & 0 & \cdots & \cdots & 0 \\ T & S & T & 0 & & \vdots \\ 0 & & & & 0 & \vdots \\ \vdots & 0 & & & & 0 \\ \vdots & & 0 & T & S & T \\ 0 & \cdots & \cdots & 0 & T & P \end{pmatrix} + \omega^2 \begin{pmatrix} M_{i1} & 0 & \cdots & \cdots & \cdots & 0 \\ 0 & M_{i1} & 0 & \cdots & \cdots & 0 \\ 0 & 0 & M_{i2} & 0 & \cdots & 0 \\ \vdots & & & \ddots & & \vdots \\ 0 & \cdots & \cdots & 0 & M_{i_{N_y}} & 0 \\ 0 & \cdots & \cdots & 0 & 0 & M_{i_{N_y}} \end{pmatrix}, \tag{A3}$$

with

$$P = \begin{pmatrix} -2k_1 - k_2 & 0 \\ 0 & -k_1 - k_2 \end{pmatrix},$$

$$S = \begin{pmatrix} -2k_1 - k_2 & 0 \\ 0 & -2k_1 - k_2 \end{pmatrix},$$

and

$$T = \begin{pmatrix} 0 & 0 \\ 0 & k_1 \end{pmatrix}.$$

The blocks of $\tilde{\mathbf{D}}$, which connect the sample region to the waveguides, are not modified by defects. They are given by

$$D_{LM} = V_{\text{up}}, \quad D_{RM} = V_{\text{down}}, \tag{A4}$$

$$D_{ML} = (\vec{D}_{ML}^{(1)}, \ldots, \vec{D}_{ML}^{(2N_y)}) \quad \text{where} \quad \vec{D}_{ML}^{(\nu)} = \kappa_\nu V_{\text{down}} \cdot \vec{u}'_\nu, \tag{A5}$$

$$D_{MR} = (\vec{D}_{MR}^{(1)}, \ldots, \vec{D}_{MR}^{(2N_y)}) \quad \text{where} \quad \vec{D}_{MR}^{(\nu)} = \kappa_\nu V_{\text{up}} \cdot \vec{u}_\nu, \tag{A6}$$

$$D_{LL}=(\vec{D}_{LL}^{(1)},\ldots,\vec{D}_{LL}^{(2N_y)})$$

$$\text{where}\quad \vec{D}_{LL}^{(\nu)}=\kappa_\nu(V_{\text{auto}}+\kappa_\nu V_{\text{down}}+\omega^2\mathbf{1})\cdot\vec{u}'_\nu, \tag{A7}$$

$$D_{RR}=(\vec{D}_{RR}^{(1)},\ldots,\vec{D}_{RR}^{(2N_y)})$$

$$\text{where}\quad \vec{D}_{RR}^{(\nu)}=\kappa_\nu(V_{\text{auto}}+\kappa_\nu V_{\text{up}}+\omega^2\mathbf{1})\cdot\vec{u}_\nu. \tag{A8}$$

Here we have used the notation $\vec{u}_\nu=\vec{u}(\kappa_\nu)$ and $\vec{u}'_\nu=\vec{u}(1/\kappa_\nu)$.

Finally, the inhomogeneous terms of Eq. (10) read

$$\vec{F}=\frac{1}{\kappa_{\overline{\nu}}}\left(V_{\text{auto}}+\frac{1}{\kappa_{\overline{\nu}}}V_{\text{down}}+\omega^2\mathbf{1}\right)\cdot\vec{u}_{\overline{\nu}}, \tag{A9}$$

$$\vec{G}=\frac{1}{\kappa_{\overline{\nu}}}V_{\text{down}}\cdot\vec{u}_{\overline{\nu}}. \tag{A10}$$

The corresponding equations for spring defects are obtained in a similar manner. However, in this case, all block matrices containing the new spring constants have to be changed, and the resulting equations cannot be written in a general compact form.

[1] For an extensive discussion see *Mathematical Physics in One Dimension*, edited by E. H. Lieb and D. C. Mattis (Academic, New York, 1966).

[2] R. Landauer, IBM J. Res. Dev. **1**, 223 (1957); Philos. Mag. **21**, 863 (1970); Z. Phys. B **68**, 217 (1987); J. Phys. Condens. Matter **1**, 8099 (1989).

[3] M. Büttiker, Phys. Rev. Lett. **57**, 1761 (1986).

[4] E. Tekman and P. F. Bagwell, Phys. Rev. B **48**, 2553 (1993).

[5] C. Berthod, F. Gagel, and K. Maschke, Phys. Rev. B **50**, 18 299 (1994).

[6] A. Khater, N. Auby, and D. Kechrakos, J. Phys.: Condens. Matter **4**, 3743 (1992).

[7] For a review see J. P. Toennies, J. Vac. Sci. Technol. A **5**, 440 (1987).

[8] T.E. Feuchtwang, Phys. Rev. **155**, 731 (1967).

[9] J. Szeftel and A. Khater, J. Phys. C **20**, 4725 (1987).

[10] L. Landau and E. Lifshitz, *Théorie de l'Elasticité* (Mir, Moscow, 1967), p. 146.

[11] H. Grimech and A. Khater, Surf. Sci. **323**, 198 (1995).

[12] Y. Pennec and A. Khater, Surf. Sci. Lett. **348**, L82 (1996).

[13] F. Gagel and K. Maschke, Phys. Rev. B **52**, 2013 (1995).

[14] M. Guglielmi, F. Montauti, L. Pellegrini, and P. Arcioni, IEEE Trans. Microwave Theory Technol. **43**, 1911 (1995).

[15] D. Marcuse, in *Quantum Electronics—Principles and Applications*, edited by P. F. Liao and P. L. Kelley (Academic, New York, 1991).